# Test results for the V0 detector in ALICE

B. Cheynis, L. Ducroux, J.-Y. Grossiord, A. Guichard, Philippe Pillot, B. Rapp, R. Tieulent, R. Alfaro, A.D. Becerril, E. Belmont-Moreno, et al.

▶ **To cite this version:**

B. Cheynis, L. Ducroux, J.-Y. Grossiord, A. Guichard, Philippe Pillot, et al.. Test results for the V0 detector in ALICE. 2003, pp.15. in2p3-00021595

**HAL Id: in2p3-00021595**
**https://hal.in2p3.fr/in2p3-00021595**

Submitted on 17 Dec 2003

**HAL** is a multi-disciplinary open access archive for the deposit and dissemination of scientific research documents, whether they are published or not. The documents may come from teaching and research institutions in France or abroad, or from public or private research centers.

L'archive ouverte pluridisciplinaire **HAL**, est destinée au dépôt et à la diffusion de documents scientifiques de niveau recherche, publiés ou non, émanant des établissements d'enseignement et de recherche français ou étrangers, des laboratoires publics ou privés.

ALICE/03-??
Internal Note/???
3 November 2003

# Test results for the V0 detector in ALICE

B. Cheynis, L. Ducroux, J.-Y. Grossiord, A. Guichard, P. Pillot, B. Rapp, R. Tieulent

*IPN-Lyon, IN2P3-CNRS et Université Claude Bernard, Lyon-I, France*

R. Alfaro, A. D. Becerril, E. Belmont-Moreno, G. Herrera⋆, A. Martínez-Davalos, A. Menchaca

*Instituto de Fisica,UNAM A.P. 20364, 01000, Mexico City, Mexico*

⋆*Centro de Investigación y de Estudios Avanzados, Mexico City 07000, Mexico*

**Abstract**

In this report, we describe the V0 detector, a device made of two arrays of scintillating counters (V0L and V0R) installed on both sides of the ALICE interaction vertex. The light yield and the time resolution were measured for several prototype counters which were tested on the PS T10 beam line and with cosmic rays. Results from the tests and from simulations are reported.

# 1 Introduction

The V0 detector is a small angle detector made of two array systems (V0R and V0L) installed on both sides of the ALICE interaction vertex [1,2]. It has multiple roles. It provides:

- a minimum bias trigger for the central barrel detectors,
- a centrality indicator,
- two centrality triggers in Pb-Pb collisions,
- a control of the luminosity,
- a validation signal for the dimuon trigger [3] to filter the large background mainly expected in the case of collisions with protons.

The evaluations of the performance of the V0 detector concerning these several points are (or will be) reported elsewhere (Physics Performance Report, Technical Design Report and Notes). In this note, we present instrumental aspects of the development carried out over the past few years which should help to choose the final system design.

The important role attributed to this device in ALICE requires to choose a robust and reliable system which has to provide a very fast time response, smaller than 25 ns. Moreover, the arrays have to be as large as possible for a good pseudo-rapidity coverage and as thin as possible along the beam directions, due to the very tight spaces available inside the L3 magnet.

A scintillating counter (SC), one of the best tools to fulfill the above requirements, is proposed as detection element for the arrays. The scintillation light will be converted by wavelength shifting (WLS) fibers and transported to a photo-multiplier (PMT) through clear (CL) fibers. A similar technique was adopted for calorimetry [4–6], multiplicity [7,8], and time [9] measurements in several other experiments. The present proposal is based on some of these works [10,11] and on some specific simulations and experimental tests.

# 2 Location and acceptance

The locations of V0L and V0R arrays are indicated in Fig. 1. The V0L array is located in the opposite direction of the dimuon spectrometer relative to the vertex, at a distance of 350 cm. Its pseudo-rapidity acceptance ranges from $\eta$ = 5.1 to $\eta$ = 2.8 and covers the full azimuthal angle. Its diameter is 86 cm. It is mounted inside a rigid box in the central part of the PMD system. This box will be part of a common mechanical structure holding the T0 and the FMD counters, a structure which is to be precisely defined. The V0R array is fixed on the dimuon spectrometer side at about 87 cm from the interaction point. Its pseudo-rapidity acceptance ranges from $\eta$ = -3.8 to $\eta$ = -1.7. Its diameter is 65 cm. It covers the spectrometer acceptance ($\Delta\eta$ = -3.8/-2.5) as well as the FMD acceptance ($\Delta\eta$ = -3.8/-1.7) over the full azimuthal angle.

The segmentation of V0L/V0R arrays is shown in Fig. 2. It is a collection of 72 elementary counters distributed according to 5 rings. Each of these rings covers 0.5-0.4 unit of pseudo-rapidity and is divided in 12 sectors of 30° azimuthal acceptance. The elements of the outer ring (ring 5) are divided in two identical detectors for an optimized signal uniformity and a

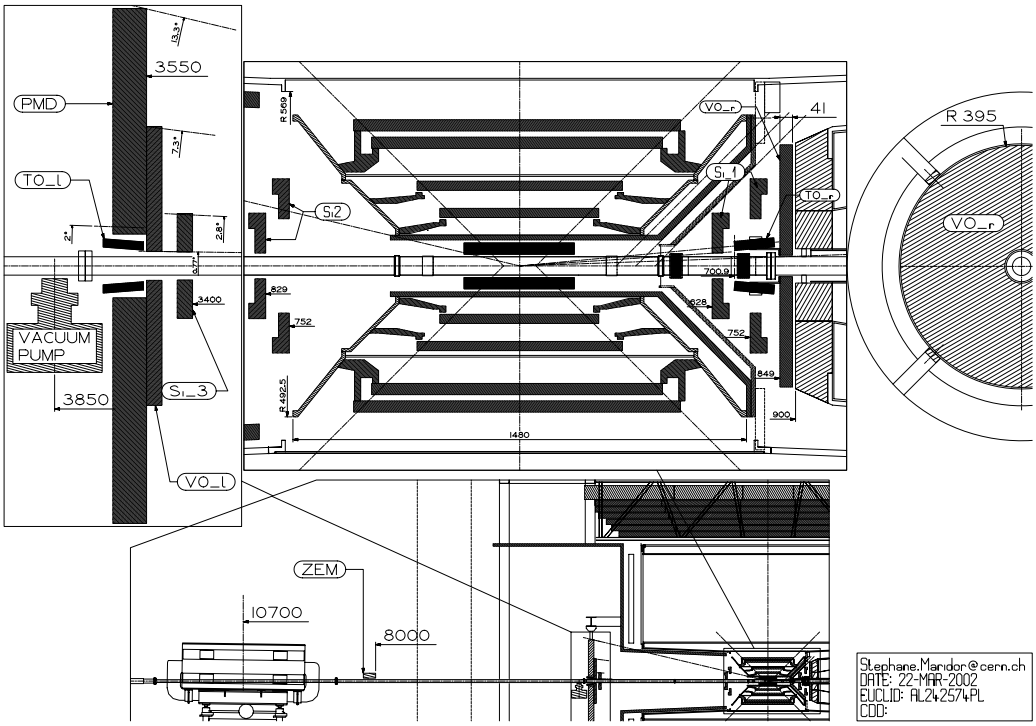


Figure 1: Layout of the V0R/V0L detector.

smaller time fluctuation. The pseudo-rapidity and angular acceptances of each ring are given in Table 1.

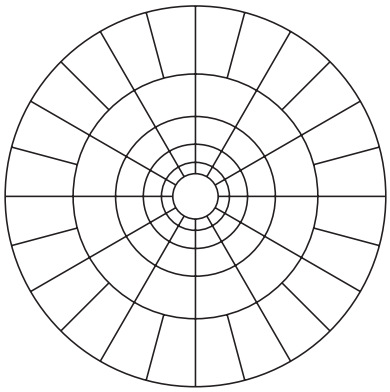

Figure 2: Segmentation of the V0 arrays.

In pp collisions, the mean number of charged particles within 0.5 unit of pseudo-rapidity is about 4. Each V0 channel will be mostly fired by only one charged particle. A very high efficiency for the detection of one MIP is thus required for a reliable multiplicity measurement in this case. Moreover, the use of the full V0 detector as filter of the background in the case of minimum bias trigger, on the one hand, and the use of the three inner V0R rings as validation device for

| Ring | V0L | | V0R | |
|---|---|---|---|---|
| | $\eta_{max}/\eta_{min}$ | $\theta_{min}/\theta_{max}$ | $\eta_{max}/\eta_{min}$ | $\theta_{min}/\theta_{max}$ |
| 1 | 5.1/4.6 | 0.7/1.2 | -3.8/-3.4 | 177.4/176.2 |
| 2 | 4.6/4.2 | 1.2/1.7 | -3.4/-2.9 | 176.2/173.7 |
| 3 | 4.2/3.7 | 1.7/2.8 | -2.9/-2.5 | 173.7/170.6 |
| 4 | 3.7/3.2 | 2.8/4.7 | -2.5/-2.1 | 170.6/166.0 |
| 5 | 3.2/2.8 | 4.7/7.0 | -2.1/-1.7 | 166.0/159.3 |

Table 1: V0L and V0R arrays. Pseudo-rapidity and angular acceptance (deg.) of the rings.

the dimuon trigger, in the other hand, reinforce this last requirement. In Pb-Pb reactions, the number of MIPs within a similar pseudo-rapidity range can go up to 4000, namely 330 MIPs per channel. Therefore, each channel has to provide a dynamics of 1-330 MIPs.

# 3 Tests of elements

## 3.1 Material, geometry, assemblage

The main requirements for the elementary channel of the V0 arrays are:

- a high and uniform light yield from the one minimum ionization particle (MIP),
- a time resolution of the order of 1 ns for the MIP,
- a large dynamics for charged particle multiplicity,
- a low intrinsic noise.

Experimental works were (and are being) especially dedicated to reach these requirements. First tests were carried out to determine the light yield from a set of SC/WLS fiber samples shaped according to a 30° sector of a V0R array as shown in Fig. 3. Scintillator pieces (BC408 or BC404 from Bicron [12]) of different thicknesses (≈10 or ≈20 mm) equipped with double cladding WLS fibers (Y11 from Kuraray [13] or BCF92 from Bicron) of two diameters (1.0 and 1.2 mm) were used. The choice of these scintillating materials was mainly motivated by their fast decay constants (3-7 ns) required for providing fast signal. Two different geometrical setups were tested. The first one (setup A) was made of 8-2 WLS fibers embedded within parallel grooves machined in one of the frontal sides of the pieces as shown in Fig. 4. The second one (setup B) was made of 8 fibers embedded along each lateral surface (total of 16 fibers) of the scintillators as shown in Fig. 5. The length of the fibers was about 40 cm long to transport the light up to the photomultiplier. An aluminium reflector was set at the end of the fibers, opposite to the PMT. Due to the small size of the counters and the minimum bending diameter recommended for the fibers, no circular groove was considered.

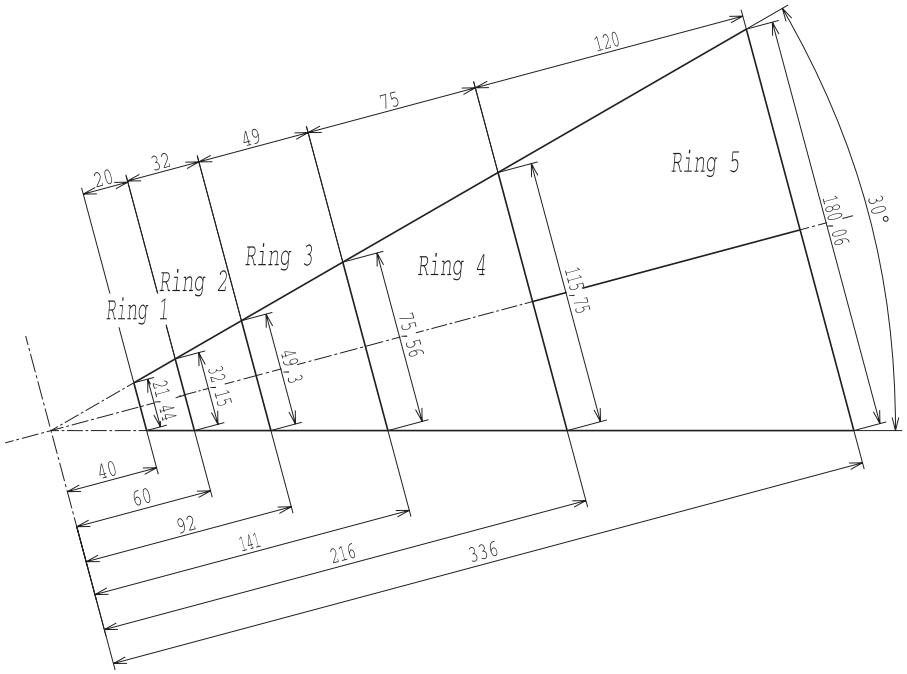


Figure 3: Dimensions of the V0R counters used for the tests.

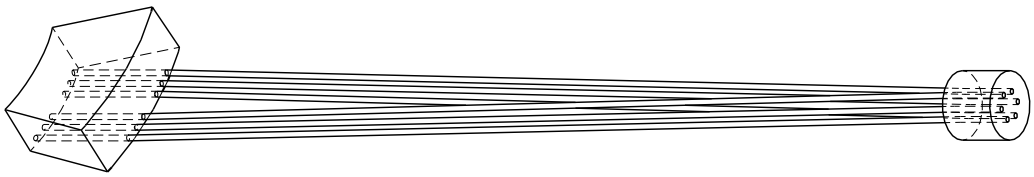

Figure 4: Elementary counter with fibers embedded along one of the frontal side of the scintillator piece (setup A).

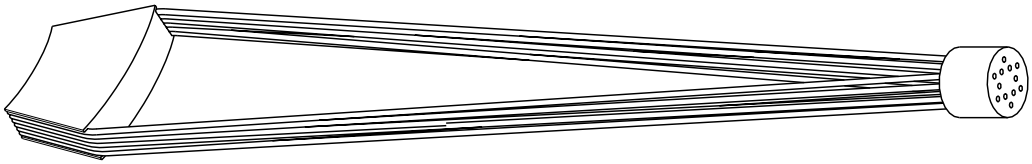

Figure 5: Elementary counter with the fibers embedded along two lateral faces of the scintillator piece (setup B).

For the V0L array the segmentation (setup C) was made using the megatile construction method [14] and [15]. The disc of plastic scintillator will be subdivided into two parts to allow its mounting on the experimental area without dismounting the beam line.

In the megatile technique a large piece of scintillator, in this case a whole semi-ring, is machined with a router most of the way through its depth in order to separate one sector from the rest. The grooves are filled with $TiO_2$ loaded epoxy to give a good optical insulation from the adjoining sectors, as well as to restore the mechanical strength. The outer surfaces of the megatile are also covered with an efficient reflector. In order to collect the light within each detection pixel, several radial grooves are machined to be filled with wavelength shifting optical fibers. These fibers run radially towards the outer edge of the megatile where they are coupled to clear fibers using optical connectors (see Fig. 6).

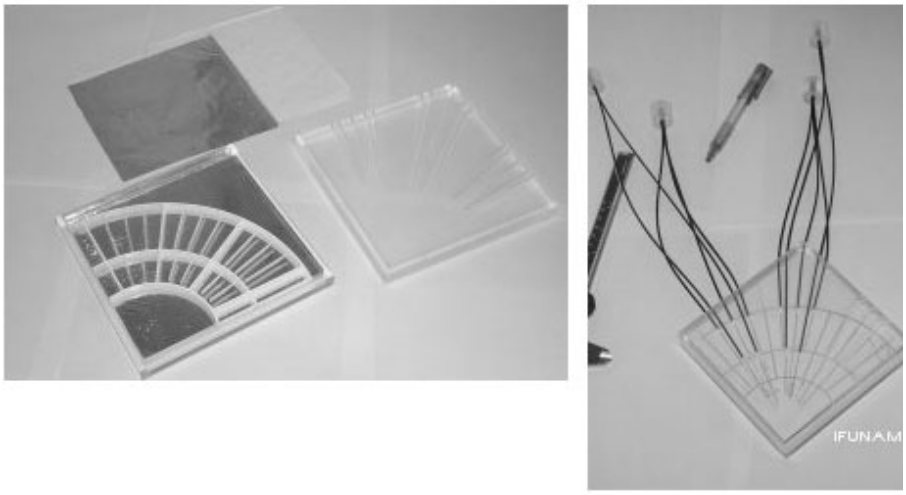


Figure 6: Proposed detector assembly (setup C).

## 3.2 Test bench

Test bench was used in the T10 beam line and for cosmic ray detection. It was equipped with XP2020 photo-multipliers from Philips Photonics [16]. Four such detectors were coupled to 12 x 14 x 0.3 $cm^3$ scintillating counters. They provided the trigger and the time reference to measure the light and the time distributions given by V0 element prototypes. Charge and time were recorded using the ADC V465 (270 pC for 4096 channels) and the TDC V488 (25 ps per channel) from CAEN [17]. The calibration of the V0 scintillating channels was obtained with a pulse generator signal exciting a light emission diode (LED) set in front of the photo-cathode of each PMT. The generator pulse level was properly adjusted so that the LED light extracts mainly one photo-electron (p.e.) from the photo-cathode. As illustration, Fig. 7(left) shows a typical distribution of the p.e. amplified charge expressed in channels of the ADC converter. It points at the channel 140, i.e. 36 channels above the pedestal. Figure 7(right) shows the charge distribution given by MIPs from the beam particles. This distribution is provided by an element

of the ring 2 made of BC408 scintillator plate 20 mm thick and BCF92 fibers with a diameter of 1 mm. The peak position, fitted with a gaussian distribution, is measured at channel number 890, i.e. 786 channels above the pedestal. It corresponds to 22 p.e. with a fluctuation value $\sigma_{p.e.} = 6$ or, expressed in MIP, $\sigma_{MIP} = 0.27$.

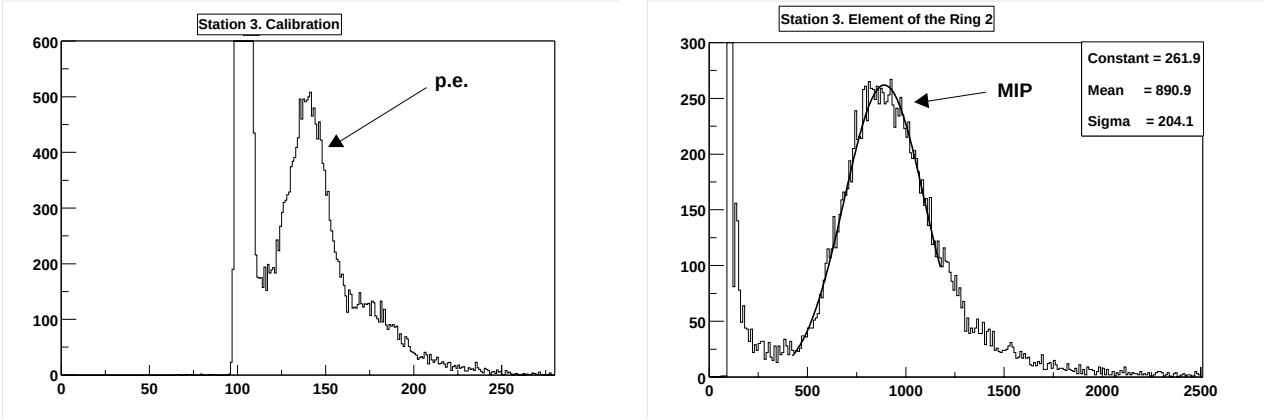


Figure 7: Charge distributions provided by a XP2020 photo-multiplier from the one photo-electron (left) and from the one MIP (right) through a counter of the ring 2.

## 3.3 Setup A

### 3.3.1 Light production from beam tests

The first tests with setup A elements were carried out with the BC600 optical cement from Bicron to fix the fibers at the bottom of the grooves and to fill the grooves. The SC/WLS fiber ensembles were covered with the titanium dioxide BC620 reflector paint from Bicron. The results obtained during the year 2001 on the PS T10 beam line delivering 7 GeV/c pion beam are presented in Table 2. It gives results obtained from several measurements in unit of photo-electron. Despite possible effects due to disparity in the mechanical mounting of the elements, several observations can be made. The light provided by the Bicron WLS fibers does not significantly depend upon their diameter. For the same scintillator thickness, the Y11 fiber is about twice as efficient as the BCF92 fiber. The $\sigma_{MIP}$ values are respectively close to 1/5 and 1/4. Furthermore, an increase of the scintillator thickness does not provide a similar increase of the collected light. Finally, the larger the tested sample, the smaller the collected light when the number of fibers remains constant. That seems to be an effect of the light attenuation inside the scintillating material.

The light attenuation in the BCF98 clear fiber from Bicron was measured. We glued 10.5 meters of this optical fiber to the end of the five WLS fibers of a ring 3 counter. The measurement of the transmitted light in this condition was performed as well as after removing 10 meters of the fibers. The attenuation value was deduced from the comparison between the two measurements. A reduction of about a factor 2 was found, in accordance with the manufacturer specifications.

| V0R sector | BC408 scint. | WLS fibers | | Y11 1.2 mm | BCF92 1.0 mm | BCF92 1.2 mm |
|---|---|---|---|---|---|---|
| | th. (mm) | nbr. | l. (mm) | p.e. $^{\sigma_{p.e.}}_{\sigma_{MIP}}$ | p.e. $^{\sigma_{p.e.}}_{\sigma_{MIP}}$ | p.e. $^{\sigma_{p.e.}}_{\sigma_{MIP}}$ |
| ring 1 | 10 | 5 | 95 | | | $16\ ^{5}_{.31}$ |
| | 20 | 5 | 95 | $59\ ^{12}_{.20}$ | $26\ ^{7}_{.27}$ | $27\ ^{7}_{.26}$ |
| ring 2 | 20 | 5 | 185 | $52\ ^{10}_{.19}$ | $22\ ^{6}_{.27}$ | |
| ring 3 | 20 | 11 | 682 | | | $31\ ^{7}_{.23}$ |
| | | 5 | 310 | $34\ ^{7}_{.21}$ | $19\ ^{6}_{.32}$ | |

Table 2: Results of tests of V0 scintillating elements coupled with wavelength shifting fibers according to setup A. The light resulting from one MIP, expressed in photo-electrons, is measured as a function of the scintillator thickness and the number, length and diameter of two kinds of fibers.

### 3.3.2 Light production from cosmic rays

In order to maximize the light provided by the V0 elements, further tests were performed in the laboratory with cosmic rays and elements of ring 3. BC600 optical cement was still used for fixing the fibers. The measurements were dedicated to the effects of several reflecting envelopes wrapping the counter. BC620 paint, Teflon film and Aluminum sheet were successively used to wrap samples made of BC404/BCF92 and BC408/Y11 scintillator/fibers couplings. The associations of such materials were motivated by the optimized matching between emission (408 and 425 nm for BC404 and BC408) and absorption (408 and 432 nm for BCF92 and Y11) wavelengths of the scintillator and the WLS fibers. The results are summarized in Table 3.

There is a confirmation of the results obtained on T10 with the BC408/Y11 counter covered by the BC620 paint, i.e. about 30 p.e.. The collected signal is about twice as large with Teflon film or Al sheet wrapping the same piece. On the contrary, the light collected with the BC404/BCF92 counter is twice as small. We must notice that taking off the reflector at the end of the fibers, opposite to the PMT, induces a loss of about 30% of the collected light. Furthermore, tests without optical glue for the embedding of the fibers within the scintillators were performed with a sample of BC408/Y11 enveloped by Teflon film. 43 p.e. were obtained showing a loss of about 24 p.e. (35%) in the produced light.

### 3.3.3 Light yield and time resolution from beam test

Tests on PS T10 using 7 GeV/c pion beam were carried out in September 2002 in order to determine the time resolution for the prototype elements of rings 1, 3, 4 and 5 (Fig. 3). For these tests, we used 1 cm thick BC408 scintillator in which Y11 WLS fibers with a diameter of 1 mm were embedded without using optical glue, contrary to the previous measurements.

| Ring 3 SC/WLS fibers 17.5/1.2 mm | SC envelope/WLS fiber end reflector | | |
|---|---|---|---|
| | BC620 paint/ BC620 paint | Teflon film/ Teflon film | Al sheet/ Al sheet |
| | Nb. of p.e. | Nb. of p.e. | Nb. of p.e. |
| BC404/BCF92 | | 35±2 | 31±3 |
| BC408/Y11 | 30±1 | 67±2 | 63±3 |

Table 3: Results of tests of V0R ring 3 scintillating elements coupled with WLS fibers according to setup A. The light obtained from cosmic rays, expressed in photo-electrons, is measured as a function of two SC/WLS fiber couplings and several types of reflecting envelopes.

In order to vary the number of detected photo-electrons, the number of embedded WLS fibers in the scintillator (as shown in Fig. 4) was changed from 8 to 2. Figure 8 shows the light yield as a function of the number of embedded WLS fibers. An important observation is the fact that the collected light does not go like the number of embedded fibers.

The time resolution for each of these configurations was measured. Its value was $\sigma_{time}^{MIP} = \sqrt{(\sigma_{meas}^2 - \sigma_{ref}^2)}$ where $\sigma_{meas}$ and $\sigma_{ref}$ were the measured and the reference (485 ps) values respectively. Figure 9 shows the results as a function of the corresponding light yield. Results from each ring were fitted by a function of the form $p_1/\sqrt{N} + p_2$, where $p_1$ and $p_2$ are free parameters of the fit and $N$ is the number of photo-electrons. The parameter $p_2$ takes into account the intrinsic time dispersion inside each scintillator element which is only function of the geometry of the element.

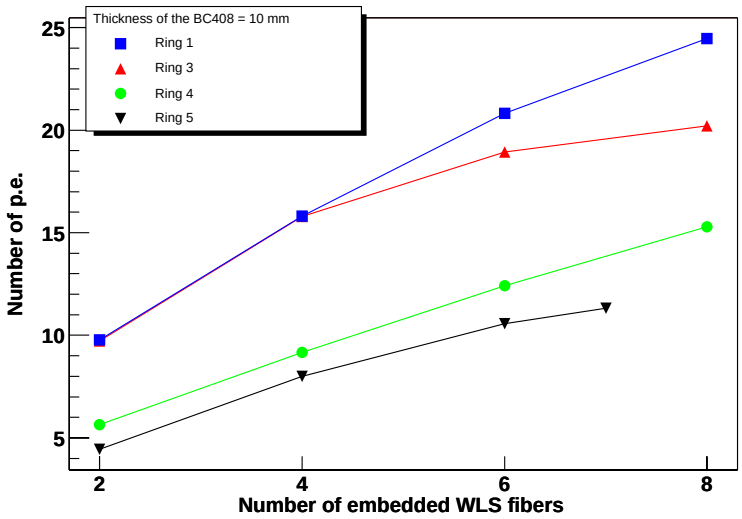


Figure 8: Number of detected photon-electrons as a function of the number of embedded WLS fibers.

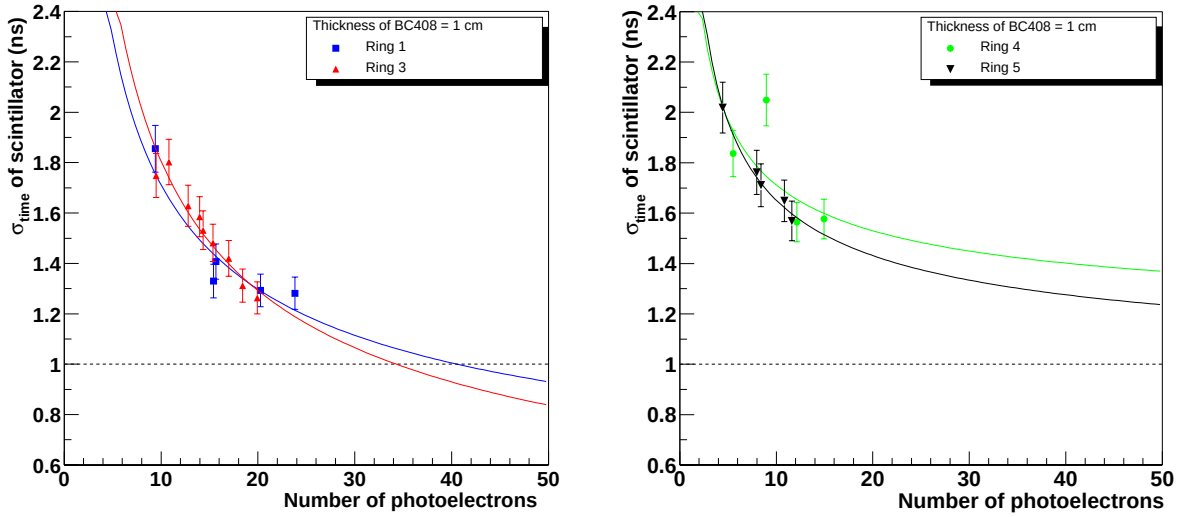


Figure 9: Time resolution as a function of the light yield for rings 1 and 3 (left) and rings 4 and 5 (right). Fitting functions are $p_1/\sqrt{N} + p_2$, where $p_1$ and $p_2$ are free parameters of the fit and $N$ is the number of photo-electrons.

As we can see in Fig. 9(left) for rings 1 and 3 and Fig. 9(right) for rings 4 and 5, the best time resolution is obtained from 8 embedded fiber configurations. It is about 1.2 ns for rings 1 and 3, and about 1.6 ns for rings 4 and 5. As mentionned in Section 3, a time resolution of about 1 ns is required in order to ensure a good background rejection. The present fits show that, in order to satisfy this condition, the number of photo-electrons should be multiplied by a factor of about 2 for rings 1 and 3 and at least a factor 5 for rings 4 and 5. It is not possible to gain such factors just by adding more WLS fibers in the scintillator. In fact, when more and more fibers are added, the number of photo-electrons saturates (see Fig. 8).

## 3.4 Setup B

Tests of the setup B (Fig. 5) with cosmic rays were carried out in the laboratory for elements of rings 4 and 5. Two 40 cm long beams of 8 WLS fibers were embedded along each lateral side (total of 16 fibers) of a 10 mm thick scintillator. Results are shown in Fig. 10 and compared to results from setup A. Light yields of 29-33 p.e. ($\sigma_{MIP}$ = MIP/5) correlated to time resolutions $\sigma_{time}^{MIP}$ of about 1.2 ns are measured with elements of ring 4 and 5 (without glue for fixing the fibers). These values should be compared to 12-15 p.e. and 1.6 ns as obtained by the setup A configuration. When using glue to fix the fibers, light yield increases up to 42 p.e. and provides a $\sigma_{time}^{MIP}$ value of 1.0 ns from the ring 4 element. Notice that addition of new measured points gives better constraints to the fitted curves which is modified as compared to the curve in Fig. 9(right). The time resolution obtained from these two largest elements seems to be the best we can reach taking into account their transverse dimensions which provide large intrinsic time dispersion inside the scintillator. Any light quantity produced by more than one MIP will give a time resolution $\sigma_{time}$ smaller than $\sigma_{time}^{MIP}$. Finally, a measurement with a 2 cm thick ring 4 prototype with glued fibers gives a light yield of 76 p.e. and a time resolution of 0.9 ns.

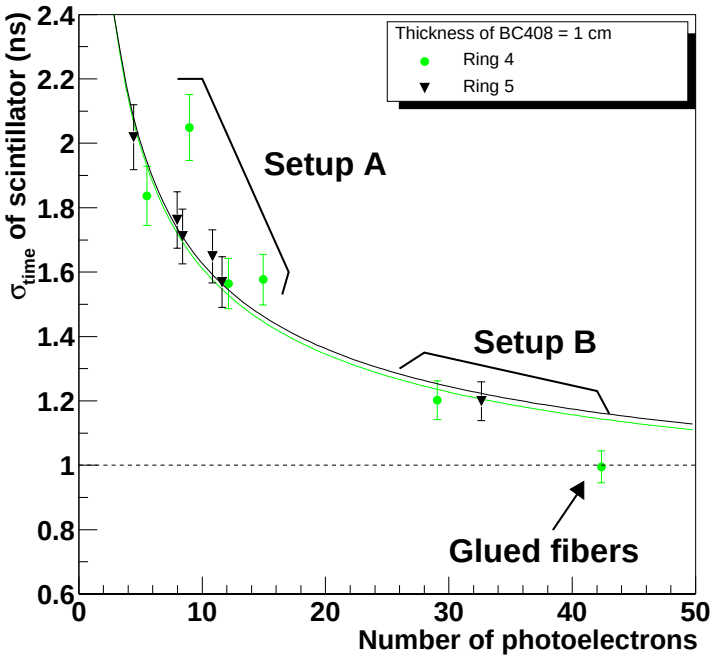


Figure 10: Time resolution as a function of the light yield for rings 4 and 5. Fitting functions are $p_1/\sqrt{N} + p_2$, where $p_1$ and $p_2$ are free parameters of the fit and $N$ is the number of photo-electrons.

These studies show clearly that the setup B is much more favorable than the setup A. A larger light quantity and a better time resolution will provide a better efficiency and a larger selectivity for the detection of the MIP.

## 3.5 Setup C

We tested the prototype made with the megatile technique. This prototype is a quarter of the whole detector. It consists of 6 segments, 3 of each belonging to the two inner rings. The number of embedded WLS fibers in the scintillator was two for the elements of ring 1, and three for the elements of ring 2.

We were interested in testing several reflecting wrappings for the scintillator; we also wanted to determine the time response of the prototype.

Once outside the scintillator, each one of the WLS fibers was covered with teflon film to avoid losses of light and black tape to prevent the entrance of external light. And also, the embedded end of the WLS fiber was covered with a reflector; in this case we used BC620 paint. We did not use optical glue to fix the fibers.

Table 4 lists the results of the tests of the V0L elements coupled with different WLS fibers and using two different wrappings. We observe that the highest signal is obtained with the Y11 fibers and Teflon film.

| V0L sector | Area of scintillator $cm^2$ | BC408 scint. wrapping | Number of WLS fibers | Y11 p.e. $\pm$ $\sigma_{p.e.}$ | BCF92 p.e. $\pm$ $\sigma_{p.e.}$ |
|---|---|---|---|---|---|
| Ring 1 | 7.99 | Aluminum | 2 | 16 $\pm$ 5 | 9 $\pm$ 4 |
| | | Teflon | 2 | 23 $\pm$ 6 | 14 $\pm$ 5 |
| Ring 2 | 18.85 | Aluminum | 3 | 19 $\pm$ 5 | — |
| | | Teflon | 3 | 30 $\pm$ 7 | — |

Table 4: Results of tests of V0L elements coupled with wavelength shifting fibers according to setup C. The light provided from one MIP, expressed in photo-electrons is measured as a function of the number of two kinds of fibers and of the scintillator wrapping.

As can be seen, with our prototype we can collect around 30 p.e. by using three fibers reading. Therefore, we expect to increase the light collection just by adding more fibers.

The time resolution of each segment was measured as well. In table 5 we report the time resolution of each element according to its light yield. Our results are similar to those obtained with V0R elements.

| V0L Sector | WLS fiber | Light Yield (number of p.e.) | Time Resolution (nsec) |
|---|---|---|---|
| Ring 1 | Kuraray Y11 | 16 $\pm$ 5 | 1.3 |
| | | 23 $\pm$ 6 | 1.3 |
| | BCF92 | 9 $\pm$ 4 | 1.1 |
| | | 14 $\pm$ 5 | 1.1 |
| Ring 2 | Kuraray Y11 | 19 $\pm$ 5 | 1.4 |
| | | 30 $\pm$ 7 | 1.4 |
| | BCF92 | — | — |
| | | — | — |

Table 5: Time resolution of each scintillating element according to its light yield.

It is clear from Table 5, that although BCF92 WLS fibers yield less photoelectrons than the Y11 WLS fibers, the best time resolution is obtained with the former ones. This, in part, is due to the intrinsic decay times of the fibers, which, according to [11] are 2.4 $\pm$ 0.4 ns for BCF92 and 8.8 $\pm$ 1.5 ns for Y11. On the other hand, as mentioned before, the association BC408/Y11 is better than BC408/BCF92 because of the matching between emission and absorption wavelengths of the scintillator and the WLS fibers. Thus, there must be a compromise between the light collection and timing requirements. We consider, therefore, very important to test again the

combination BC404/BCF92 as well as BC408/Y11 and so try to obtain an even balance of light yield and time response.

On the basis of the results presented in this report, we are now able to propose a new design for V0L. Starting off from the present model, we have decided to construct another prototype with the megatile technique, but using more WLS fibers per segment. With this, we expect to obtain a better light collection and time resolution. Therefore, we consider necessary to test this new model, which could cover the established requirements.

# 4 Simulations

Simulation of the optical response of the V0 elements were performed in order to optimize the output signal. The simulation is based on the package LITRANI developed for the CMS experiment. LITRANI is a C++/ROOT program which allows to generate and propagate optical photons from their emission point to a detecting device through optical materials as complex as birefringent anisotropic media [18]. There are several choices of initial photon distributions. Among other possibilities, the photons can be created by particles crossing material according to different processes (dE/dx energy loss, Čerenkov emission, electromagnetic cascade, etc...).

In order to propagate photons, the program takes into account the geometry and the optical parameters of the different media used in the device, such as refractive indices, absorption, diffusion and scattering lengths, reflection and diffusion coefficients, photo-cathode quantum efficiency. LITRANI takes care of wavelength dependences if required.

Using LITRANI, we simulated the response of V0 elements to a beam of 7 GeV/c pions. In fact, we calculated the number of scintillation photons coming upon any fiber of the detector. No absorption and emission functions, neither transmission acceptance of the WLS fiber to PMT are taken into account. Nevertheless, the number of photons at the level of the fibers should be proportional to the light collected at the end of the fibers. Only their distributions should be narrower. The results, presented in Fig. 11 for setup A, are normalized on the experimental measurement provided by the ring 1 element coupled to 8 fibers, namely 25 p.e. as reported in Fig. 8. Then, numbers of p.e. given by simulations below correspond to setups without use of optical glue. The open squares and open triangles correspond respectively to 6 and 8 WLS fiber configurations. A systematic error of 5% was assigned to the results in order to take into account possible errors due to approximations in the geometry description. We reported on the same figure (filled markers) the light yield measured during the test beam for the similar configurations. We can observe that the simulation is in relatively good agreement with the test beam results except for the largest element which shows a discrepancy of about 40%.

Table 6 gives the results obtained by the simulation for the two different setups realized without using optical glue. Here are given the number of expected photo-electrons in front of the PMT. Setup A gives a photo-electron yield variation of about 1.7 between elements of rings 1 and 4. This last effect is not so large with the setup B. A gain of a factor 1.6 and 2.2 is recorded with setup B and elements of rings 1 and 4. Moreover, an increase of a factor 1.7 is obtained when the scintillator thickness is doubled. If glue is used to fix the fibers, another factor 1.3 should be applied to the numbers of the Table 6.

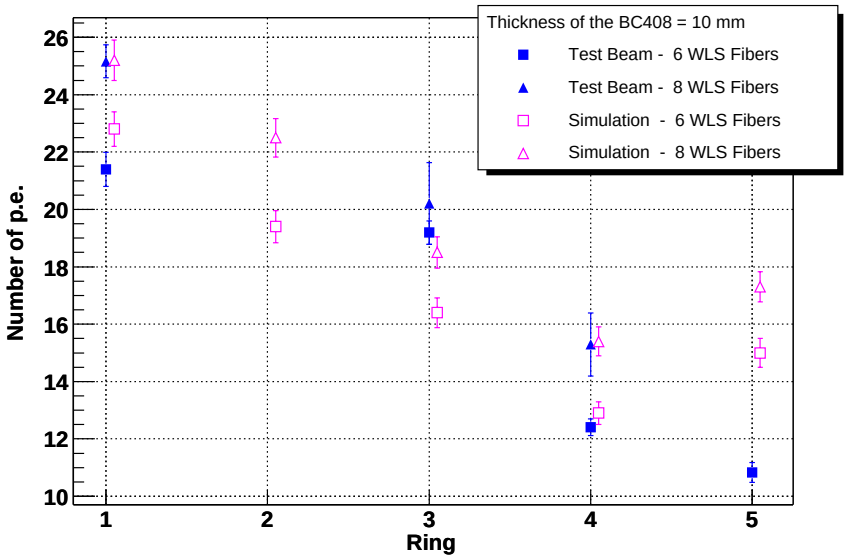


Figure 11: Comparison between results obtained during the test beam (filled symbols) and results of the simulation (open symbols). Light yield as a function of the ring number of the element.

| Ring | Setup A (10 mm) | Setup B (10 mm) | Setup B (20 mm) |
|---|---|---|---|
| 1 | 25 | 41 | 69 |
| 2 | 23 | 40 | 67 |
| 3 | 19 | 36 | 61 |
| 4 | 15 | 33 | 56 |
| 5 | 17 | 32 | 54 |

Table 6: Number of photon-electrons from V0R elements according to setups A (8 fibers) and B.

In order to characterize the response of the detector in the configuration of each setup, we mapped the efficiency of photon detection on the entire surface of elements. Figure 12 shows, for setup A, the number of photons captured by fibers as a function of the impact point of the particle on the surface of a ring 4 element (left) and their distribution (right). This figure shows clearly that the photon collection is inhomogeneous. The efficiency is good in the fiber localization but decreases rapidly as the impact point moves away from them. The larger the distance, the smaller the probability for a photon to be transmitted to a fiber with few reflections on the scintillator surface. Therefore, the detection efficiency is dropping off away from the fibers. In particular, small signals are obtained from impacts in the most distant corners.

Figure 13 shows, for setup B, the number of photons recorded by the fibers as a function of the impact point on the element (left) and their distribution (right). The effects associated to impacts in the corners of the scintillator for setup A disappear. Moreover, the light collection is much larger (by a factor 2.2) and more uniform.